Photofragment coincidence imaging of small $I^-(H_2O)_n$ clusters excited to the charge-transfer-to-solvent state

David E. Szpunar, Kathryn E. Kautzman, Ann Elise Faulhaber, and Daniel M. Neumark*

Department of Chemistry, University of California, Berkeley, California 94720, and Chemical Sciences Division, Lawrence Berkeley National Laboratory, Berkeley, California 94720

Abstract

The photodissociation dynamics of small $I^-(H_2O)_n$ (n=2-5) clusters excited to their charge-transfer-to-solvent (CTTS) states have been studied using photofragment coincidence imaging. Upon excitation to the CTTS state, two photodissociation channels were observed. The major channel (~90%) is a 2-body process forming neutral I + $(H_2O)_n$ photofragments, and the minor channel is a 3-body process forming I + $(H_2O)_{n-1}$ + H_2O fragments. Both process display translational energy ($P(E_T)$) distributions peaking at E_T=0 with little available energy partitioned into translation. Clusters excited to the detachment continuum rather than to the CTTS state display the same two channels with similar $P(E_T)$ distributions. The observation of similar $P(E_T)$ distributions from the two sets of experiments suggests that in the CTTS experiments, I atom loss occurs after autodetachment of the excited $[I(H_2O)_n^-]^*$ cluster, or, less probably, that the presence of the excess electron has little effect on the departing I atom.

* Corresponding author. Electronic mail: dneumark@berkeley.edu

I Introduction

Anions in polar solvents display a broad absorption band in the UV, assigned to the transfer of the excess charge from the anion to the solvent.[1] As these charge-transfer-to-solvent (CTTS) states are an excellent means of production of the solvated electron,[2] they have been the subject of many studies in the literature. In particular, solvated iodide has been the focus of many time-resolved studies probing the dynamics of the CTTS process.[3-7] The solvent[8] and temperature effects[9] on the dynamics have also been investigated. These condensed phase studies have motivated work on $X^-(H_2O)_n$ clusters (X = F, Cl, Br, I) as a means to examine how an intrinsically bulk phenomenon, namely CTTS excitation and electron solvation, manifests itself in finite clusters. As a result, $X^-(H_2O)_n$ clusters have been subject to many studies.[10] In particular, the dynamics of $I^-(H_2O)_n$ clusters excited to their CTTS states have been the focus of numerous theoretical and experimental studies. Prior experimental studies[11-15] of the CTTS dynamics of $I^-(H_2O)_n$ clusters have used femtosecond pump-probe spectroscopy to investigate the short-time dynamics of these species. The work detailed here focuses on the asymptotic dynamics of these clusters, in which photofragment coincidence imaging determines the product channels, translational energy distributions, and angular distributions of $I^-(H_2O)_{n=1-5}$ clusters excited to their CTTS states.

Although there was initially some controversy as to the location of the iodide anion,[16-18] the current consensus is that the iodide resides on the surface of the water cluster even in larger clusters.[19-24] The ground state geometries of smaller clusters have recently been calculated by Lee and Kim.[21] For $I^-(H_2O)_{n=3,4}$ clusters, the water molecules are predicted to form a cyclic structure supported by hydrogen bonds, with all of the

"free" H atoms pointing upwards to the iodide anion forming ionic hydrogen bonds in a crown-like configuration. $I^-(H_2O)_5$ is predicted to have several low-lying structures, the lowest energy geometry of which is a four-membered ring once again forming ionic bonds with the iodide anion and the fifth water branching off forming an ionic hydrogen bond with the iodide.

Binding energies of $I^-(H_2O)_n$ clusters have been determined through photoelectron spectroscopy (PES) studies,[16,25,26] and calculations[27,28] are in good agreement with the experimental determinations. Tentative assignments were made to neutral $I(H_2O)$ modes using zero electron kinetic energy (ZEKE) spectroscopy.[29] Johnson and coworkers[30-35] have obtained infrared spectra of several $X^-(H_2O)_n$ clusters using Ar predissociation spectroscopy. The vibrational and electronic spectroscopy of $I^-(H_2O)_n$ clusters have also been investigated theoretically.[20-22,36]

The above studies have yielded a fairly detailed picture of the ground states of these clusters. The first gas phase measurement of their electronic spectroscopy was performed by Serxner et al.,[37] who recorded action spectra of $I^-(H_2O)_{n=0-4}$ clusters and identified the cluster analog to the CTTS state in clusters with as little as two waters. The spectra showed a broad absorption over the detachment continuum characteristic of a dipole-bound state, in which the dipole moment of the water cluster is significant enough to bind the excited electron.[38] Several studies have calculated the CTTS states of $I^-(H_2O)_n$ clusters in good agreement with the spectra of Serxner et al.[36,39-41]

Neumark and coworkers examined the excitation of small $I^-(H_2O)_n/(D_2O)_n$ clusters (n = 4-6) excited to the cluster analog of the CTTS state using femtosecond photoelectron spectroscopy (FPES).[11,12] Photoelectron spectra were recorded after a

~100 fs pump pulse (4.71 eV) excited the clusters to the CTTS state, and a probe pulse of 1.57 eV detached the electron after a variable delay time. $I^-(H_2O)_4$ clusters showed simple population decay, while n = 5, 6 clusters showed a steady increase in electron binding energy (decrease in electron kinetic energy) after several hundred femtoseconds. These spectral shifts were interpreted as evidence for electron solvation, as water rearrangement to stabilize the excess electron would result in an increase in binding energy. This interpretation was subsequently challenged in a theoretical study by Chen and Sheu,[42,43] who proposed that the time-dependent shifts in the PE spectra were due to iodine atom detachment from the cluster rather than from solvent rearrangement. Subsequent theoretical work by Peslherbe,[44] Jordan,[45] and Kim[46-50] suggested that both solvent and I atom motion played a role in the early-time dynamics of CTTS states in clusters. More recent time-resolved photoelectron imaging experiments[14,15] on larger $I^-(H_2O)_n$ clusters support the interpretation of the early-time increase in electron binding energy in terms of solvation dynamics.

Nonetheless, the role of the I atom in the overall dynamics of these clusters is of considerable interest. The time-resolved experiments by Kammrath et al.[14] on $I^-(H_2O)_n$ ($n \leq 10$) clusters excited at 4.67 eV showed early (~1 ps) spectral shifts assigned to solvent reorganization and, for clusters with five or more water molecules, a later shift toward higher electron binding energy, occurring between 25 and 75 ps, attributed to loss of the I atom. These experiments also yielded the time scale for autodetachment from the excited clusters, a process that can be identified by its extremely slow photoelectrons, yielding autodetachment lifetimes ranging from 0.6 to 324 ps for n = 3-7. Comparison of all the observed time scales implies that I atom loss occurs prior to autodetachment for clusters

with n>5 and that both process occur on the same time scale for n=5. The absence of an observable I atom shift for clusters with $n < 5$ suggests that autodetachment occurs before the I atom leaves in these small clusters, since once the excited state decays, the photoelectron imaging experiment can no longer follow its dynamics. This interpretation of the dynamics in the smallest clusters differs somewhat from recent theoretical studies by Kim[50] that propose the repulsive interaction between the excess electron and the I atom induces I atom loss prior to autodetachment.

In this paper, we perform complementary experiments on the excited state dynamics of $I^-(H_2O)_n$ ($n \leq 5$) clusters that focus on their asymptotic dynamics in order to determine, for example, if the I atom actually does leave the excited cluster and if so, how much energy it carries away and what happens to the remaining water cluster. Using our fast beam coincidence imaging apparatus, we characterized the dissociation channels of excited $I^-(H_2O)_n$ clusters, measuring the photofragment masses for 2- and 3-body dissociation, the amount of energy partitioned to photofragment translation, and the angular distributions of the photofragments. These experiments were performed at the CTTS excitation energies for clusters with n=2-5, and also at higher excitation energies in the direct detachment continuum. We found only neutral photofragments to be produced. The major channel at both sets of excitation energies was loss of an I atom, while a minor 3-body channel producing neutral I, $(H_2O)_{n-1}$ and H_2O was also found. The photofragment translational energy distributions in both sets of experiments were quite similar and showed very little translational energy release. These results imply that upon CTTS excitation, either autodetachment occurs before I atom loss, or that the excess electron has little effect on the departing I atom.

II Experimental

The fast beam coincidence imaging apparatus, shown in Fig. 1, has been described in detail elsewhere, and will only be briefly described here. [51-53] An $I^-(H_2O)_n$ cluster beam was formed by first flowing neat Ar at a pressure of ~20 psi over CH_3I, bubbling the resulting Ar/CH_3I mixture through water, followed by a supersonic expansion through a pulsed piezoelectric valve operating at 60 Hz. An electron beam (1 keV) directed perpendicularly to the expansion was used as an ionization source. The resulting cluster anions were accelerated to 4.5 keV and mass-selected using a Bakker time-of-flight mass spectrometer. Ions of the desired mass intersected the frequency-doubled light from an excimer (Lambda Physik LPX 210, 308 nm) pumped dye laser (Lambda Physik Scanmate 2E) at the CTTS maxima (3.9 eV, 4.2 eV, 4.4 eV, 4.7 eV for n = 2, 3, 4, 5 clusters respectively).[37] Laser energies of 0.5-1 mJ/pulse were used. The resulting photofragments then traveled the 2.15 m flight length and struck a time-and-position-sensitive (TPS) detector. The fragments from each dissociation event were detected in coincidence; the arrival times and positions of the fragments were then used to calculate the masses of the fragments as well as fragment velocities. Thus, collection of many coincident images enabled the calculation of a translational energy distribution, $P(E_T)$, as well as the anisotropy parameter $\beta(E_T)$ that specifies the photofragment angular distribution.[54]

The TPS detector, based on the design by Zajfman and co-workers,[55] comprises a standard imaging quality 75 mm Z-stack micro channel plate (MCP) coupled to a phosphor screen (Burle Spec. S9739, Rev. 0). A beam splitter was positioned at a 45° angle to the phosphor screen, transmitting roughly half of the phosphorescence to an

image intensifier and a CCD camera (Dalsa, CA-D6-D512), yielding position information. The remaining phosphorescence was reflected to a 4x4 photomultiplier (PMT) array (Hamamatsu H 6568-10) giving precise timing and crude position information. Correlation of the CCD and PMT signals yielded timing and position for all photofragments from each photodissociation event. One can directly detect both anionic as well as neutral fragments with this setup, making it ideally suited to study the $I^-(H_2O)_n$ system. As will be seen, all the products detected were neutral, so a pulsed field (~200 V) was used to deflect any of the undissociated parent ions away from the detector, as shown in the inset of Fig. 1. As a result, the beam block used in all previous experiments on this instrument was unnecessary.

III Results

Figure 2 (black lines) shows the 2-body photofragment mass distributions for the $I^-(H_2O)_{n=2\text{-}5}$ clusters excited to their CTTS states. The photon energies used were 3.9 eV, 4.2 eV, 4.4 eV, 4.7 eV for n = 2,3,4,5 respectively, based on the spectra of Serxner et al.[37] Although the experimental CTTS maximum for $I^-(H_2O)_5$ is not known, the photon energy used, 4.7 eV, should be very close to the maximum and, due to the width of the CTTS peak, will still excite the n = 5 cluster to the CTTS state. Data for $I^-(H_2O)$, also shown in Figure 2, were collected at the arbitrary energy of 4.4 eV, as there is no CTTS resonance for this cluster size.[37] Each mass distribution shows two peaks corresponding to the $(H_2O)_n$ (n×18 amu) and I (127 amu) fragment. As mentioned in the experimental section, the data presented here were taken with a pulsed field applied after the dissociation laser was fired, in order to deflect any undissociated parent ions away from

the detector. Data sets taken with and without the deflecting field were identical. This identifies the products as neutral, corresponding to the asymptotic dissociation process $I^-(H_2O)_n \rightarrow I\,(^2P_{3/2}) + (H_2O)_n + e^-$. ($I\,(^2P_{1/2})$ formation is not energetically allowed.)

Figure 3 shows the experimental $P(E_T)$ distributions for all clusters, as well the anisotropy parameter, $\beta(E_T)$, for the n=3-5 clusters. As can be seen, all cluster sizes partition little energy into translation, with nearly all the translational energy release below 0.1 eV, and display an isotropic photofragment angular distribution with $\beta=0$. The lack of translational energy imparted in the dissociation of the n = 1,2 clusters, along with the large mass ratio of the photofragments (127:18 and 127:36) prevented many of the fragments from receiving enough recoil velocity perpendicular to the beam axis to "clear" a dead spot on the center of the detector. For this reason the $P(E_T)$ distributions shown for $I^-(H_2O)_{n=1,2}$ are "raw" distributions, not corrected for the detector acceptance function, which calibrates for the geometric factors that prevent the collection of all of the dissociation events.[56] As a result, anisotropy parameters for the dissociation were not calculated.

Our photofragment coincidence imaging technique allows the detection of 3-body dissociation. Such a channel was found for the n = 2-5 cluster sizes excited to their CTTS states, and the corresponding photofragment mass distributions are shown in Figure 4 (black lines). For each cluster, the 3-body channel corresponds to the fragments H_2O (18 amu), $I\,(^2P_{3/2})$ (127 amu) and $(H_2O)_{n-1}$ ($(n-1)\times18$ amu). Once again, the products were found to be neutral, corresponding to the reaction $I^-(H_2O)_n \rightarrow I + (H_2O)_{n-1} + H_2O + e^-$. Figure 5 shows the $P(E_T)$ distributions calculated from the 3-body dissociation data. Just as in the 2-body channel, little energy is partitioned into translation. A rough

estimate of the branching ratio for the 2-body channel to the 3-body channel is ~6:1, 10:1, 11:1, 14:1 for n = 2,3,4,5 clusters respectively. These are upper bounds, however, since the detection efficiency of the photofragments is less than unity, making it less likely to detect all fragments in coincidence from a 3-body event compared to a 2-body event.

Figure 6 displays Dalitz plots[57] for the 3-body dissociation channels. These plots show the partitioning of momentum to the photofragments from 3-body dissociation. Each point represents the fraction of the square of momentum of each 3-body photofragment event, $P_j^2 / \sum P_j^2$, with all points lying within an inscribed circle as required by momentum conservation. The Dalitz plot for $I^-(H_2O)_2$ is symmetric about the line representing equal partitioning of momentum into the two water molecules, as the H_2O fragments are indistinguishable.[58] Most of the points in this plot correspond to $P_I^2 / \sum P_j^2 > 0.5$. For the larger clusters, the Dalitz plots show that relatively little momentum is partitioned to the H_2O fragment, with most of the points corresponding to $P_{H_2O}^2 / \sum P_j^2 < 0.25$. As n increases, the fraction of momentum for the $(H_2O)_{n-1}$ fragment increases slightly at the expense of that for the I atom.

Data were also taken for n = 3-5 excited at 5.6 eV, which is considerably to the blue of the respective CTTS resonances. At this photon energy, one probes the dissociation dynamics from the neutral internal energy distribution corresponding to direct detachment of the anion, i.e. the Franck-Condon distribution typically obtained in photoelectron spectroscopy. Once again, the same two channels were observed. The 2-body mass distributions of the 5.6 eV data (dashed line) are shown plotted alongside the CTTS mass distributions (black line) in Figure 2. The resolution of the mass

distributions at 5.6 eV is considerably worse. The $P(E_T)$ distributions are shown in Figure 3; photofragment angular distributions (not shown) were isotropic. Note that the $P(E_T)$ distributions resulting from CTTS excitation and direct detachment are very similar, with only slightly more translational energy appearing in the latter.

The 5.6 eV 3-body mass distributions are shown in Figure 4, plotted with those taken at the respective CTTS states (black line). Here, however, the mass resolution of the two data sets are similar. The poor statistics of the 3-body channel at 5.6 eV, where the absorption cross section is considerably lower than on resonance,[37] prevented the calculation of a meaningful $P(E_T)$ distribution.

IV Discussion

In this section we consider the dissociation dynamics from CTTS excitation and direct detachment in more detail. There are two main channels observed when $I^-(H_2O)_{n=2-5}$ clusters are excited to their CTTS states:

$$I^-(H_2O)_n + h\nu_{CTTS} \rightarrow I(^2P_{3/2}) + (H_2O)_n + e^- \quad (1)$$

$$I^-(H_2O)_n + h\nu_{CTTS} \rightarrow I(^2P_{3/2}) + (H_2O)_{n-1} + H_2O + e^- \quad (2)$$

As pointed out in Section III, channel (1) is the dominant process for all cluster sizes. Figure 3 shows that this dissociation channel partitions little energy into product translation with an isotropic photofragment angular distribution. The minor channel (2) forms three neutral photofragments: I, $(H_2O)_{n-1}$ and H_2O. We first examine the $P(E_T)$ distributions for channel (1) and use these to obtain a more complete picture of the overall dynamics following CTTS excitation. This is followed by a discussion of channel (2).

IV A: Dynamics of the two-fragment channels

The first step in the interpretation the $P(E_T)$ distributions is to compare them to the translational energy available to the products. For channel (1), the amount of energy available, E_{avl}, for photofragment translation, E_T, and internal excitation, E_{int}, is given by

$$E_{avl} = E_T + E_{int} = h\nu - eKE + E_{int}^{(-)} - EA(I) - D_0 \qquad (3)$$

where $h\nu$ is the photon energy, $E_{int}^{(-)}$ is the internal energy of the parent ion, taken here to be negligible, eKE is the electron kinetic energy, EA(I) = 3.059 eV is the electron affinity of iodine,[59] and D_0 is the I^-— $(H_2O)_n$ association energy. D_0 is estimated from the ΔH values for $I^-(H_2O)_n \rightarrow I^-(H_2O)_{n-1} + H_2O$ measured by Hiraoka et al.[60] and by assuming the water-water interaction for the dimer (0.21 eV[61]) is additive; values are listed in Table 1.

Eq. (3) is perfectly general and applies to both CTTS excitation and direct detachment, with the difference between the two sets of experiments reflected primary in the eKE distribution. The eKE distribution for CTTS excitation has been determined by recent photoelectron imaging experiments on $I^-(H_2O)_n$ clusters performed in our laboratory with a tunable laser; these have shown that only very slow electrons are produced at these wavelengths,[62] consistent with autodetachment as the main electron production mechanism (see below). Hence, we set eKE=0 in Eq. (3) for the CTTS experiments. This gives values of E_{avl} = 0.22, 0.54, 0.55. 0.67 eV for n = 2-5 respectively. These values are shown in Table 1.

Excitation at 5.6 eV results in direct detachment of the ion, leaving the nascent neutral with an internal energy distribution determined by the Franck-Condon overlap with the ion. The nascent neutral will then dissociate, leaving the photofragments with an available energy as defined in Eq. (3). Here, however, the eKE is not negligible, and is obtained from the vertical binding energies of Markovich et al.[25] Neglecting the spread

in eKE and substituting eKE = hν – VBE, where VBE is the vertical binding energy, into Eq. (3) gives

$$E_{avl} = VBE - EA(I) - D_0 \qquad (4)$$

where EA(I) and D_0 are defined above. This yields an available energy of 0.63, 0.74, 0.74 for n = 3-5 clusters, respectively, i.e. similar but slightly higher values than were found for CTTS excitation. These results are also tabulated in Table 1.

Although there is uncertainty in the parent beam internal energy, $E_{int}^{(-)}$, as well as in the calculation of D_0, it is clear that the observed $P(E_T)$ distributions peak at 0 eV and terminate well shy of the energetic limit, regardless of whether the $I^-(H_2O)_n$ cluster is excited to the CTTS state or the direct detachment continuum. These results suggest a statistical dissociation mechanism in both cases, which typically leads to partitioning most of the available energy into internal degrees of freedom.[63]

The next point to consider in the interpretation of these experiments is whether the electron is ejected prior or subsequent to heavy-particle fragmentation. In the case of direct detachment, electron ejection is essentially instantaneous, but if autodetachment from an excited electronic state of the anion dominates, as appears to be the case for CTTS excitation, there is a time scale associated with this process that must be compared with that for fragmentation.

For direct detachment, the internal energy distribution subsequent to electron ejection reflects the Franck-Condon overlap between the anion and the two neutral states resulting from the interaction of the $I(^2P_{3/2})$ level with the surrounding solvent species.[64,65] The *n*=1 cluster is bound by 44 meV, and the two electronic states are split by 38 meV.[29] Dissociation then occurs from neutral species on either surface with

sufficient vibrational excitation to fall apart. This excitation can be in the $I^-\cdot\cdot H_2O$ bonds, the hydrogen bonds between the water molecules, and in the water molecules themselves, depending on the geometry changes that occur upon photodetachment. We also note that any vibrational excitation in the anions can enhance formation of vibrationally excited neutrals, thereby facilitating dissociation. However, the form of the $P(E_T)$ distributions, peaking at 0 eV and dropping off rapidly with increasing E_T, strongly suggests that the initial distribution of vibrational energy does not drive the dissociation dynamics, and that instead, the internal energy of the neutral complex is randomized prior to dissociation.

For CTTS excitation, we can obtain insight into the competition between autodetachment and heavy-particle fragmentation by considering the $P(E_T)$ distributions in Fig. 3. Several theoretical papers have pointed out that subsequent to CTTS excitation of $I^-(H_2O)_n$ clusters, there should be a repulsive interaction between the I atom and excess electron that will presumably drive some of the ensuing dynamics. Our results suggest that while this effect may indeed be present, it does not result in direct dissociation of the I atom on a repulsive potential energy surface. Such a mechanism would likely result in a translational energy distribution peaking away from E_T=0 and extending more towards the maximum available translational energy. For example, recent calculations by Kim[46,50] on direct dissociation from a repulsive $[I(H_2O)_n^-]^*$ surface result in $I + (H_2O)_n^-$ photofragments with translational energy release of 0.1 eV for $n = 3$ and 0.2 eV for $n = 6$, in contrast to the observed $P(E_T)$ distributions that drop to nearly zero intensity by 0.1 eV.

The second point of interest is that the $P(E_T)$ distributions for channel (1) from direct detachment and CTTS excitation are essentially the same, with only slightly more

translational energy from direct detachment. This result is easily understood if, subsequent to CTTS excitation, autodetachment precedes I atom loss, so that the I atom is leaving from a neutral complex with slightly less internal energy than that from direct detachment. This interpretation is also consistent with the time-resolved photoelectron imaging experiments discussed in the Introduction,[14] which implied that at 4.67 eV excitation energy, autodetachment was faster than I atom loss for clusters with $n<5$, and that the rates for the two processes were comparable for the $n=5$ cluster. An alternative and, in our view, less likely explanation of the $P(E_T)$ distributions would be that autodetachment does not occur before I atom loss, but the interaction between the excess electron and I atom is sufficiently weak so that the departing I atom is not affected significantly.

Our preferred interpretation is in line with the calculations on $I^-(H_2O)_4$ by Vila and Jordan,[66] who found that relatively small changes in the solvent geometry subsequent to CTTS excitation would reduce the electron binding energy significantly, thus favoring rapid autodetachment. We note that the simulations by Peslherbe[44] and Kim[47,50] show the I atom moving away from the solvent network on a time scale faster than 1 ps. Our experiment does not necessarily contradict these calculations. It is possible, for example, that the I atom becomes trapped in a shallow minimum resulting from a combination of solvent and electronic motion; the existence of such a minimum was found in electronic structure calculations by Kim,[46] and its presence was also inferred from our time-resolved studies on larger clusters.[14]

Although detachment from the water cluster following dissociation cannot be ruled out entirely, we believe that for the clusters studied here ($n \leq 5$), autodetachment followed by dissociation is the likely mechanism responsible for channel 1:

$$I^-(H_2O)_n + h\nu_{CTTS} \rightarrow [I(H_2O)_n^-]^* \qquad (5)$$

$$[I(H_2O)_n^-]^* \rightarrow I(H_2O)_n + e^-$$

$$I(H_2O)_n \rightarrow I(^2P_{3/2}) + (H_2O)_n$$

We note that the time-resolved experiments on larger clusters ($n>5$) indicate that autodetachment is slower than I atom loss,[14] and it will be of interest to investigate the photodissociation dynamics of these clusters on the instrument used here.

IV B: Dynamics of three-fragment channels

The $P(E_T)$ distributions for the 3-fragment channel, channel (2), are similar to those of channel (1), regardless of cluster size. Based on the arguments given above, we assume autodetachment to be followed by cluster dissociation. Following autodetachment, there are several possible mechanisms for the minor 3-body decay channel, which can either be concerted (reaction 6 below) or sequential (reactions 7-8 below). The sequential dissociation would most likely occur from two possible cases: I atom loss followed by dissociation of the nascent water cluster (7), or through loss of one H_2O followed by $I(H_2O)_{n-1}$ dissociation (8).

$$I(H_2O)_n \rightarrow I(^2P_{3/2}) + (H_2O)_{n-1} + H_2O \qquad (6)$$

$$I(H_2O)_n \rightarrow I(^2P_{3/2}) + (H_2O)_n \qquad (7a)$$

$$I(^2P_{3/2}) + (H_2O)_n \rightarrow I(^2P_{3/2}) + (H_2O)_{n-1} + H_2O. \quad (7b)$$

$$I(H_2O)_n \rightarrow I(H_2O)_{n-1} + H_2O \quad (8a)$$

$$I(H_2O)_{n-1} + H_2O \rightarrow I(^2P_{3/2}) + (H_2O)_{n-1} + H_2O \quad (8b)$$

Neither the $P(E_T)$ distributions nor the Dalitz plots leads to an unambiguous assignment of the three-body channel to one of these mechanisms. However, the observation that I atom loss (1) is the dominant two-body dissociation channel strongly implies that three-body dissociation occurs sequentially via (7a) and (7b), in which some fraction of the $(H_2O)_n$ clusters have enough internal energy to lose a water molecule by evaporation. This sequential mechanism is consistent with the small amount of momentum partitioning to the H_2O fragment as revealed by the Dalitz plots.

The presence of channel (2) may explain an unusual feature of the fragment mass spectra for two-body dissociation in Fig 3, which show that the mass resolution for two-body dissociation is worse for clusters excited at 5.6 eV than that obtained from excitation to the CTTS state. This effect may result from three-body events being incorrectly counted as two-body events, which would happen, for example, if the $(H_2O)_n$ fragment falls apart with very little kinetic energy, and the corresponding two spots on the phosphor screen are focused onto the same element of the 4x4 PMT array. This scenario is reasonable to expect for channel (2), since fragmentation of the water cluster should result in very little translational energy release. It can happen using either excitation scheme. However, compared to CTTS excitation, direct detachment result in higher average internal energy in the neutral clusters, as shown in Table 1. Morever, the

photoelectron spectra of these clusters are quite broad, [16] indicating that some fraction of the neutral clusters has considerably more internal energy than indicated in Table 1. Both effects will contribute toward the enhancement of channel (2) from direct detachment, resulting in more three-body events being counted as two-body events and thereby broadening the two-body mass distribution. As to be expected, the mass distribution of $I^-(H_2O)$ is much narrower (~12 amu FWHM) compared to the CTTS data of $I^-(H_2O)_2$ (~25 amu FWHM) because there is no three-body channel available to broaden the distribution.

V Conclusions

$I^-(H_2O)_n$ clusters excited to their CTTS states show two major dissociation pathways. The major pathway (~90%) is a 2-body channel producing neutral $I(^2P_{3/2})$ + $(H_2O)_n$ fragments. The second channel is a 3-body process forming $I(^2P_{3/2})$ + H_2O + $(H_2O)_{n-1}$ (~10%). The 2-body $P(E_T)$ peaks at 0 eV and terminates well shy of the energetic limit. Clusters excited to the direct detachment continuum show qualitatively similar $P(E_T)$s, suggesting dissociation of neutral clusters when excited to the CTTS as well as to the continuum. For this reason, autodetachment of the excited clusters followed by a statistical dissociation of the nascent neutral cluster is assigned as the most likely mechanism (5). However, direct dissociation of the excited cluster followed by autodetachment of the $(H_2O)_n^-$ cluster cannot be ruled out entirely.

The minor channel, 3-body dissociation producing neutral I, $(H_2O)_{n-1}$ and H_2O is also believed to occur following autodetachment of the excited cluster. Although it is not possible to determine the mechanism of this process, the fact that I atom loss is the major

channel suggest that it is most likely that 3-body dissociation proceeds via a sequential process, where I atom ejection is followed by $(H_2O)_n$ evaporation (7).

Acknowledgments

This work was supported by the Director, Office of Basic Energy Sciences, Chemical Sciences Division of the U.S. Department of Energy under contract No. DE AC02-05CH11231.

References

[1] M. J. Blandamer and M. F. Fox, Chemical Review **70**, 59 (1970).

[2] J. Jortner, M. Ottolenghi, and G. Stein, J. Phys. Chem. **68**, 247 (1964).

[3] F. H. Long, H. Lu, X. Shi, and K. B. Eisenthal, Chem. Phys. Lett. **169**, 165 (1990).

[4] F. H. Long, X. Shi, H. Lu, and K. B. Eisenthal, J. Phys. Chem. **1994**, 7252 (1994).

[5] J. A. Kloepfer, V. H. Vilchiz, V. A. Lenchenkov, and S. E. Bradforth, Chem. Phys. Lett. **298**, 120 (1998).

[6] J. A. Kloepfer, V. H. Vilchiz, V. A. Lenchenkov, A. C. Germaine, and S. E. Bradforth, J. Chem. Phys. **119**, 6288 (2000).

[7] V. H. Vilchiz, J. A. Kloepfer, A. C. Germaine, V. A. Lenchenkov, and S. E. Bradforth, J. Phys. Chem. A **105**, 1711 (2001).

[8] V. H. Vilchiz, X. Chen, J. A. Kloepfer, and S. E. Bradforth, Rad. Phys. and Chem. **72**, 159 (2005).

[9] H. Iglev, A. Trifonov, A. Thaller, I. Buchvarov, T. Fiebig, and A. Laubereau, Chem. Phys. Lett. **403**, 198 (2005).

[10] W. H. Robertson and M. A. Johnson, Annu. Rev. Phys. Chem. **54**, 173 (2003).

[11] L. Lehr, M. T. Zanni, C. Frischkorn, R. Weinkauf, and D. M. Neumark, Science **284**, 635 (1999).

[12] A. V. Davis, M. T. Zanni, C. Frischkorn, and D. M. Neumark, J. Electron Spectrosc. and Rel. Phenom. **108**, 203 (2000).

[13] A. V. Davis, M. T. Zanni, R. Weinkauf, and D. M. Neumark, Chem. Phys. Lett. **353**, 455 (2002).

[14] A. Kammrath, J. R. R. Verlet, G. Griffin, and D. M. Neumark, J. Phys. Chem. A (in press).

[15] J. R. R. Verlet, A. Kammrath, G. Griffin, and D. M. Neumark, J. Chem. Phys. (in press).

[16] G. Markovich, S. Pollack, R. Giniger, and O. Cheshnovsky, J. Chem. Phys. **101**, 9344 (1994).

[17] J. E. Combariza, N. R. Kestner, and J. Jortner, Chem. Phys. Lett. **221**, 156 (1994).

[18] J. E. Combariza, N. R. Kestne, and J. Jortner, J. Chem. Phys. **100**, 2851 (1994).

[19] J. V. Coe, J. Phys. Chem. A **101**, 2055 (1997).

[20] J. Kim, H. M. Lee, S. B. Suh, D. Majumdar, and K. S. Kim, J. Chem. Phys. **113**, 5259 (2000).

[21] H. M. Lee and K. S. Kim, J. Chem. Phys. **114**, 4461 (2001).

[22] H. M. Lee, D. Kim, and K. S. Kim, J. Chem. Phys. **116**, 5509 (2002).

[23] D. M. Koch and G. H. Peslherbe, Chem. Phys. Lett. **359**, 381 (2002).

[24] L. X. Dang, J. Chem. Phys. **110**, 1526 (1999).

[25] G. Markovich, R. Giniger, M. Levin, and O. Cheshnovsky, J. Chem. Phys. **95**, 9416 (1991).

[26] R. Mabbs, E. Surber, and A. Sanov, J. Chem. Phys. **122**, 054308 (2005).

[27] L. X. Dang and B. C. Garrett, J. Chem. Phys. **99**, 2972 (1993).

[28] H. Gai, G. K. Schenter, L. X. Dang, and B. C. Garrett, J. Chem. Phys. **105**, 8835 (1996).

[29] C. Bassmann, U. Boesl, D. Yang, G. Drechsler, and E. W. Schlag, Int. J. Mass Spec. Ion Proc. **159**, 153 (1996).

[30] P. Ayotte, G. H. Weddle, J. Kim, and M. A. Johnson, J. Am. Chem. Soc. **120**, 12361 (1998).

[31] P. Ayotte, G. H. Weddle, and M. A. Johnson, J. Chem. Phys. **110**, 7129 (1999).

[32] P. Ayotte, S. B. Nielsen, G. H. Weddle, and M. A. Johnson, J. Phys. Chem. A **103**, 10665 (1999).

[33] P. Ayotte, G. H. Weddle, J. Kim, J. A. Kelley, and M. A. Johnson, J. Phys. Chem. A **103**, 443 (1999).

[34] E. G. Diken, J.-W. Shin, E. A. Price, and M. A. Johnson, Chem. Phys. Lett. **387**, 17 (2004).

[35] P. Ayotte, G. H. Weddle, J. Kim, and M. A. Johnson, Chem. Phys. **239**, 485 (1998).

[36] H.-Y. Chen and W.-S. Sheu, J. Am. Chem. Soc. **122**, 7534 (2000).

[37] D. Serxner, C. E. H. Dessent, and M. A. Johnson, J. Chem. Phys. **105**, 7231 (1996).
[38] K. D. Jordan and F. Wang, Annu. Rev. Phys. Chem. **54**, 367 (2003).
[39] D. Majumdar, J. Kim, and K. S. Kim, J. Chem. Phys. **112**, 101 (2000).
[40] W.-S. Sheu and Y.-T. Liu, Chem. Phys. Lett. **374**, 620 (2003).
[41] W.-S. Sheu and Y.-T. Liu, Chem. Phys. Lett. **399**, 73 (2004).
[42] H.-Y. Chen and W.-S. Sheu, Chem. Phys. Lett. **335**, 475 (2001).
[43] H.-Y. Chen and W.-S. Sheu, Chem. Phys. Lett. **353**, 459 (2002).
[44] Q. K. Timerghazin and G. H. Peslherbe, J. Am. Chem. Soc. **125**, 9904 (2003).
[45] F. D. Vila and K. D. Jordan, J. Phys. Chem. A **106**, 1391 (2002).
[46] H. M. Lee, S. B. Suh, and K. S. Kim, J. Chem. Phys. **119**, 7685 (2003).
[47] H. M. Lee and K. S. Kim, Mol. Phys. **102**, 2485 (2004).
[48] M. D. Elola and D. Laria, J. Chem. Phys. **117**, 2238 (2002).
[49] J. M. Park and H. M. Lee, Bulletin of the Korean Chemical Society **25**, 937 (2004).
[50] M. Kolaski, H. M. Lee, C. Pak, M. Dupuis, and K. S. Kim, J. Phys. Chem. A **109**, 9419 (2005).
[51] R. E. Continetti, D. R. Cyr, D. L. Osborn, D. J. Leahy, and D. M. Neumark, J. Chem. Phys. **99**, 2616 (1993).
[52] A. A. Hoops, J. R. Gascooke, A. E. Faulhaber, K. E. Kautzman, and D. M. Neumark, J. Chem. Phys. **120**, 7901 (2004).
[53] A. A. Hoops, J. R. Gascooke, K. E. Kautzman, A. E. Faulhaber, and D. M. Neumark, J. Chem. Phys. **120**, 8494 (2004).
[54] R. N. Zare, Molecular Photochemistry **4**, 1 (1972).
[55] Z. Amitay and D. Zajfman, Rev. Sci. Instrum. **68**, 1387 (1997).
[56] D. R. Cyr, Ph.D. thesis, the University of California, Berkeley (1993).
[57] R. H. Dalitz, Philosophical Magazine **44**, 1068 (1953).
[58] C. Maul and K.-H. Gericke, J. Phys. Chem. A **104**, 2531 (2000).
[59] J. E. Bartmess, in *NIST Chemistry WebBook, NIST Standard Reference Database Number 69*, edited by P. J. Linstrom and W. G. Mallard (National Institute of

Standards and Technology, Gaithersburg MD, 20899 (http://webbook.nist.gov), June, 2005).

[60] K. Hiraoka, S. Mizuse, and S. Yamabe, J. Phys. Chem. **92**, 3943 (1988).

[61] F. N. Keutsch and R. J. Saykally, PNAS **98**, 10533 (2001).

[62] A. Osterwalder, M. Nee, J. Zhou, and D. M. Neumark, in preparation.

[63] J. C. Light, Disc. Faraday Soc., 14 (1967).

[64] I. Yourshaw, Y. X. Zhao, and D. M. Neumark, J. Chem. Phys. **105**, 351 (1996).

[65] A. Sanov, J. Faeder, R. Parson, and W. C. Lineberger, Chem. Phys. Lett. **313**, 812 (1999).

[66] F. D. V. a. K. D. Jordan, J. Phys. Chem. A **106**, 1391 (2002).

n	$h\nu_{CTTS}$ *(eV)*	$E_{avl,\ CTTS}$ *(eV)*	D_0 *(eV)*	$E_{avl,5.6\ eV}$ *(eV)*
2	3.9	0.22	0.62	0.24
3	4.2	0.54	0.60	0.63
4	4.4	0.55	0.79	0.74
5	4.7	0.67	0.97	0.74

Table 1 Table showing the CTTS energy, I^-—$(H_2O)_n$ association energy (D_0), and available energy, E_{avl}, for clusters excited to the CTTS state and the continuum.

Figure captions

Figure 1: Schematic of the fast beam coincidence imaging apparatus. Detail of the interaction region showing the pulsed field used to deflect undissociated parent ions from striking the detector is also shown.

Figure 2: 2-body photofragment mass distributions of $I^-(H_2O)_{n=2-5}$ excited at 3.9, 4.2, 4.4 and 4.7 eV respectively, shown in solid line. The 2-body photofragment mass distributions of $I^-(H_2O)$ excited at 4.4 eV and $I^-(H_2O)_{n=3-5}$ excited at 5.6 eV are shown in dashed line. The distributions correspond to production of I (127 amu) and $(H_2O)_n$ (n×18 amu).

Figure 3: 2-body translational energy distributions ($P(E_T)$) of $I^-(H_2O)_{n=2-5}$ excited at 3.9, 4.2, 4.4 and 4.7 eV respectively (solid), as well as the $P(E_T)$ distributions of $I^-(H_2O)_{n=1,3-5}$ excited at 5.6 eV (dashed lines). The anisotropy parameters, $\beta(E_T)$, as a function of translational energy are also shown for n=3-5 clusters excited to their CTTS states.

Figure 4: 3-body photofragment mass distributions of $I^-(H_2O)_{n=2-5}$ excited at 3.9, 4.2, 4.4 and 4.7 eV respectively, shown in solid lines. The 3-body photofragment mass distributions of $I^-(H_2O)_{n=3-5}$ excited at 5.6 eV are shown in dashed lines. The

distributions correspond to production of I (127 amu), H_2O (18 amu) and $(H_2O)_{n-1}$ (18×(n-1) amu). The mass resolution is comparable in both cases.

Figure 5: Three-body $P(E_T)$ distributions $I^-(H_2O)_{n=2-5}$ excited at 3.9, 4.2, 4.4 and 4.7 eV respectively.

Figure 6: Dalitz plots of $I^-(H_2O)_{n=2-5}$ excited at 3.9, 4.2, 4.4 and 4.7 eV respectively, showing the partitioning of little momentum to the H_2O fragment and a near equal partitioning of momentum to the I and $(H_2O)_{n-1}$ fragments.

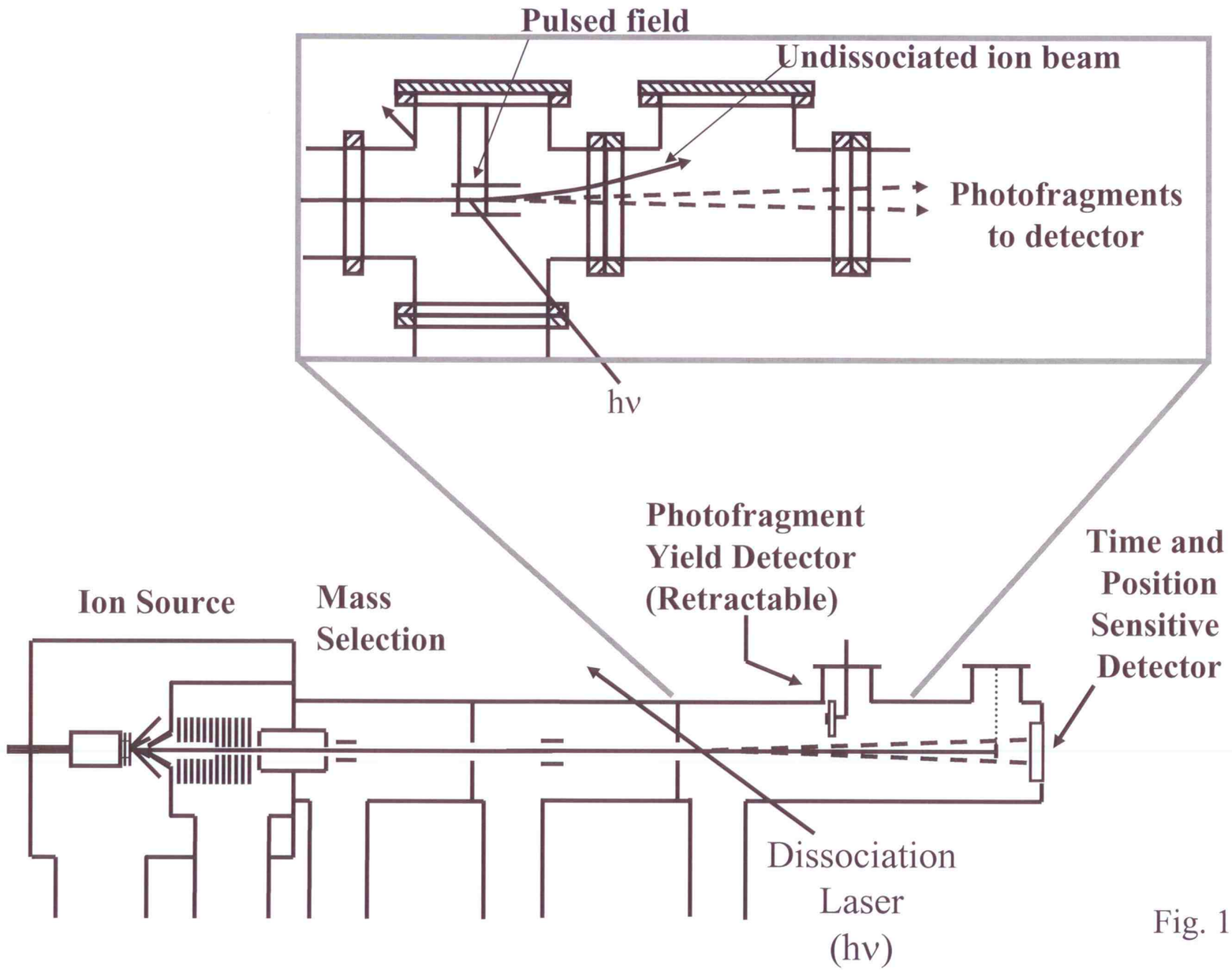
Pulsed field
Undissociated ion beam
Photofragments
to detector
hν
Photofragment
Yield Detector
(Retractable)
Time and
Position
Sensitive
Detector
Ion Source
Mass
Selection
Dissociation
Laser
(hν)

Fig. 1

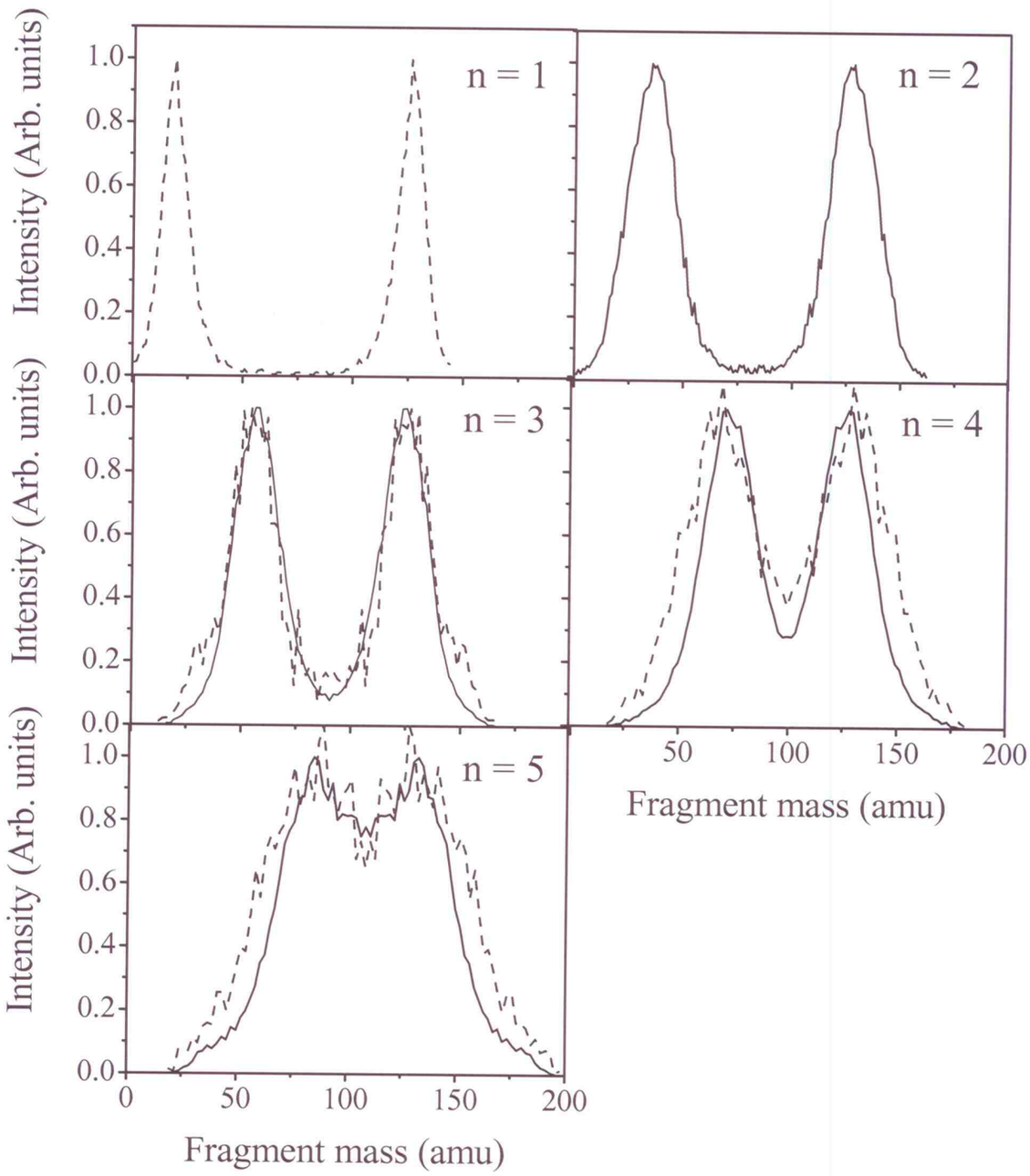
n = 1
n = 2
n = 3
n = 4
n = 5
Intensity (Arb. units)
Fragment mass (amu)
0.0
0.2
0.4
0.6
0.8
1.0
0
50
100
150
200

Fig. 2

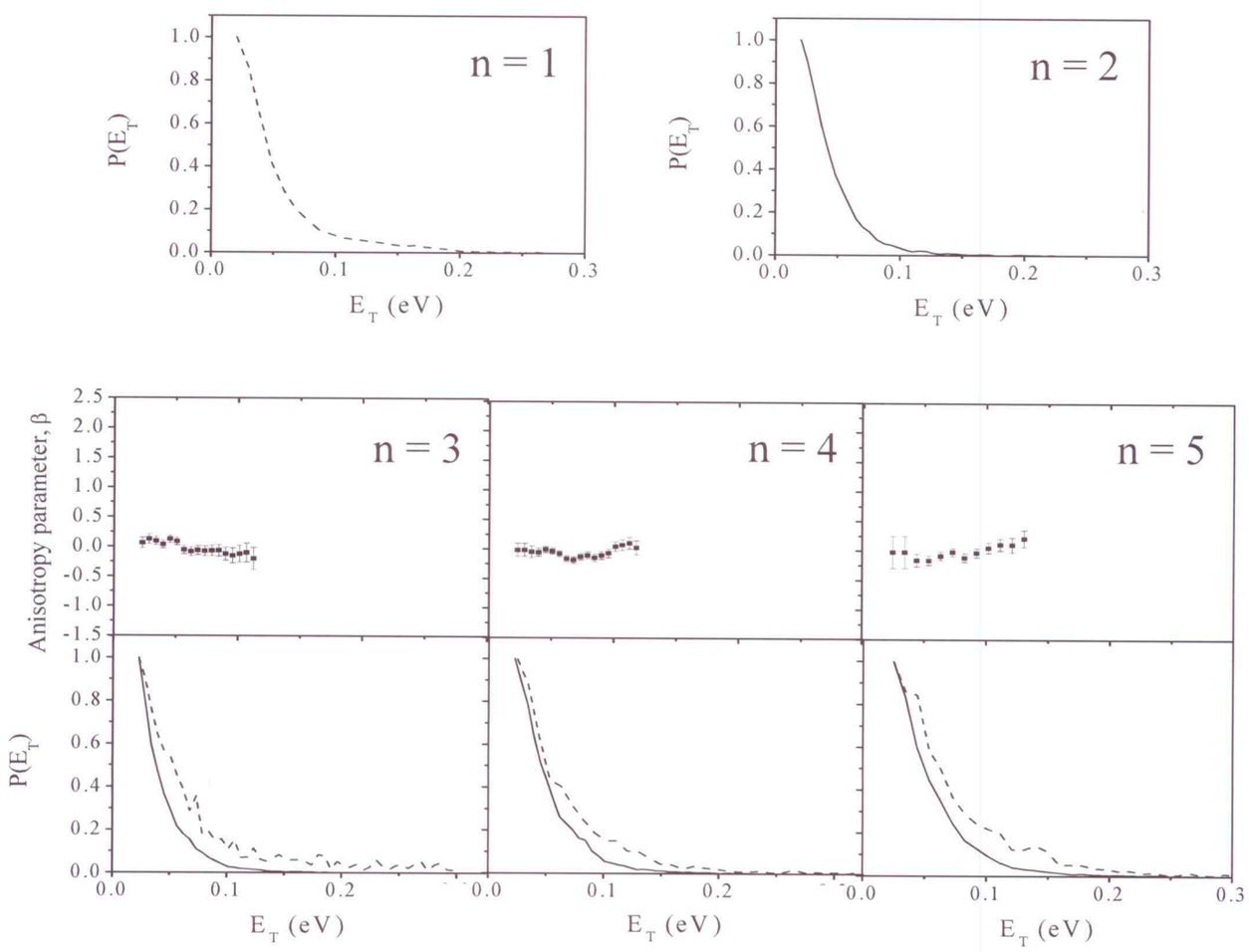

Fig. 3

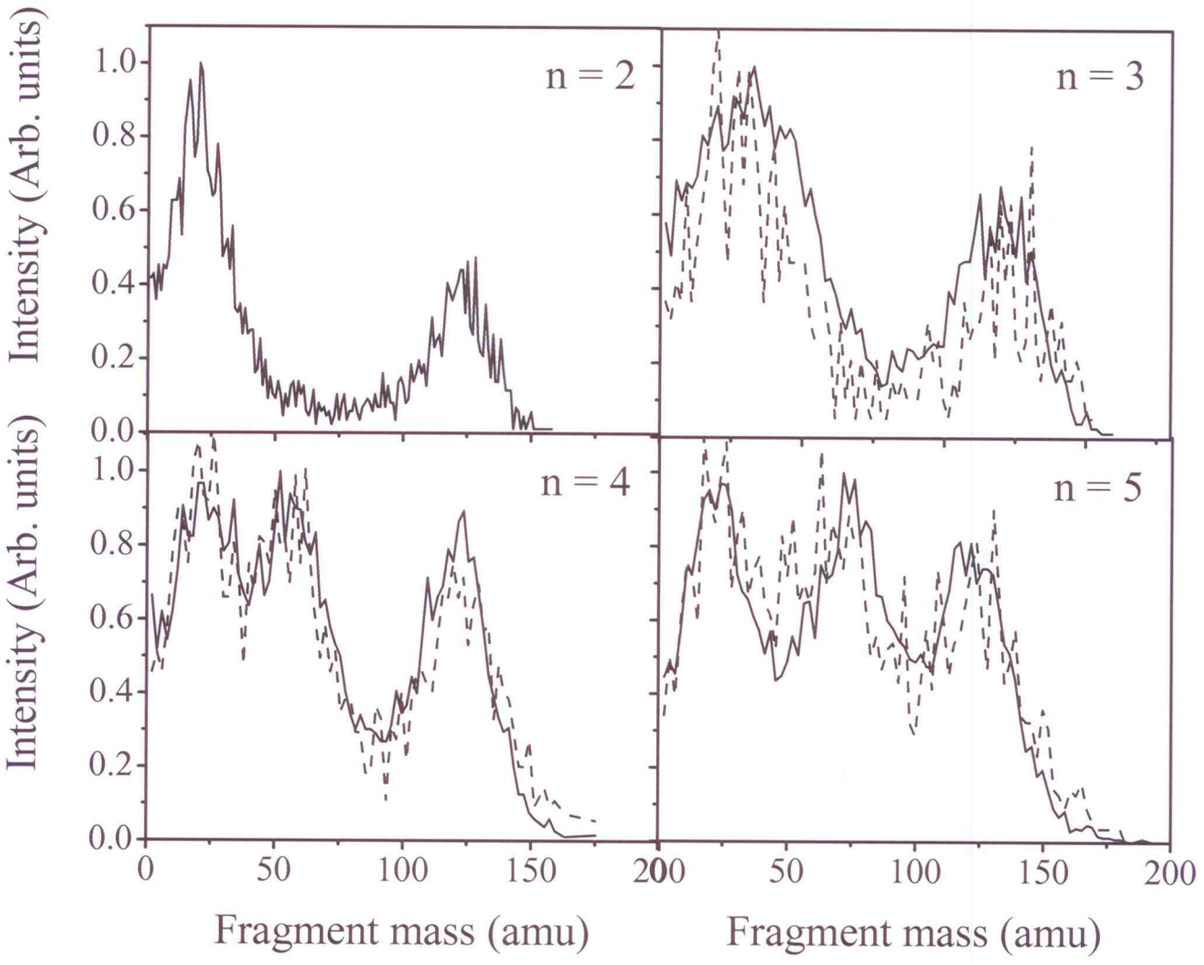
Intensity (Arb. units)
Intensity (Arb. units)
n = 2
n = 3
n = 4
n = 5
1.0
0.8
0.6
0.4
0.2
0.0
0
50
100
150
200
Fragment mass (amu)
Fragment mass (amu)

Fig. 4

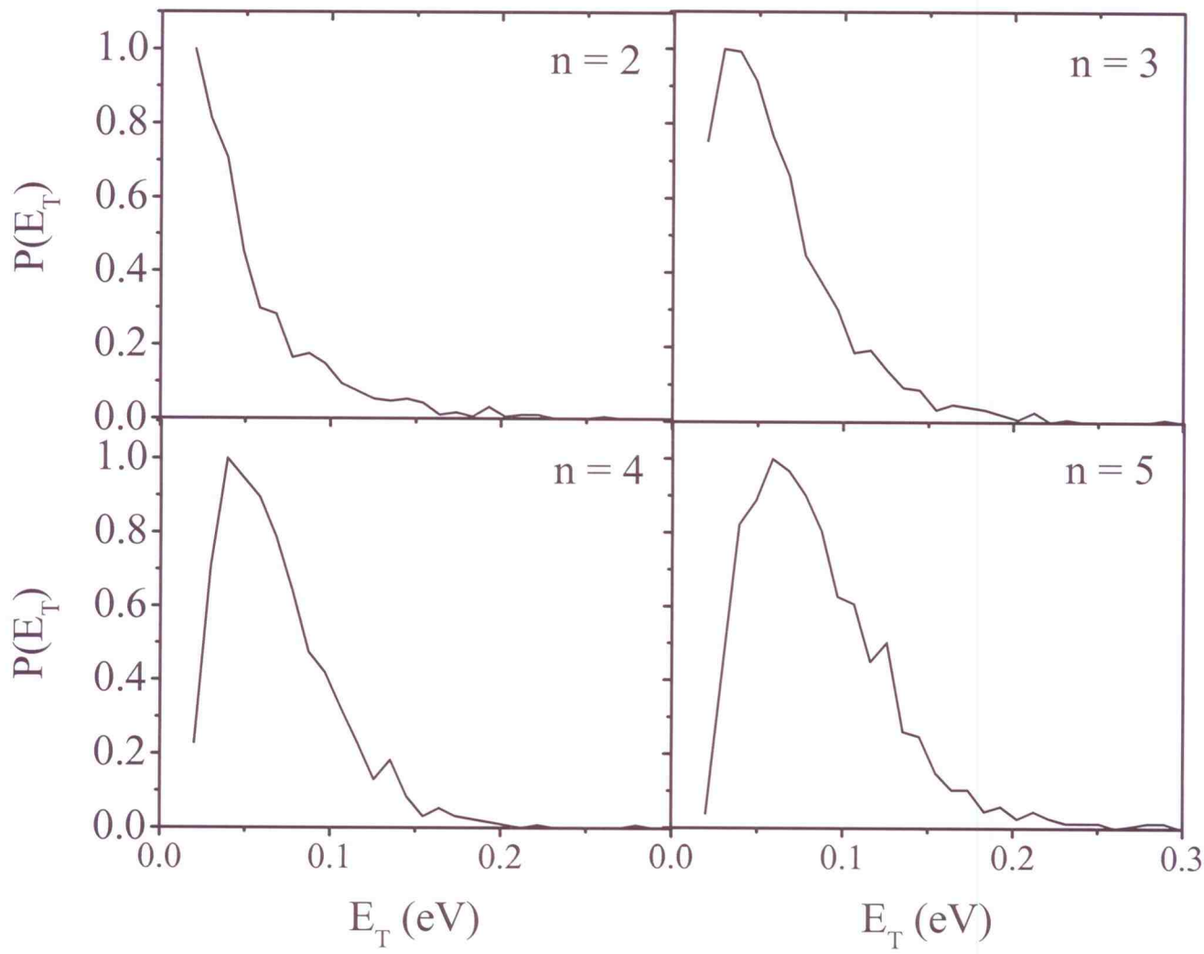

Fig. 5

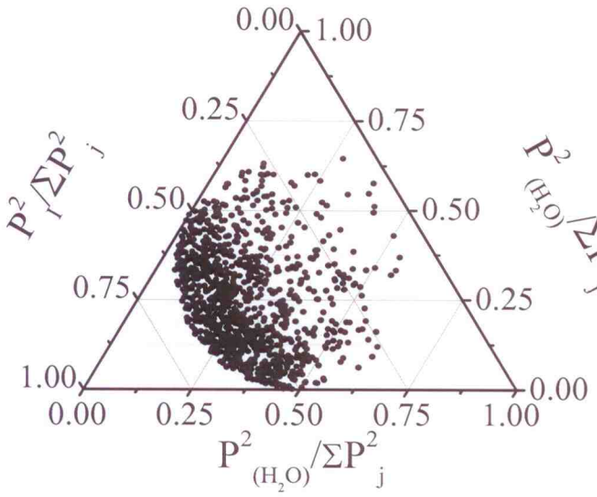

n = 2

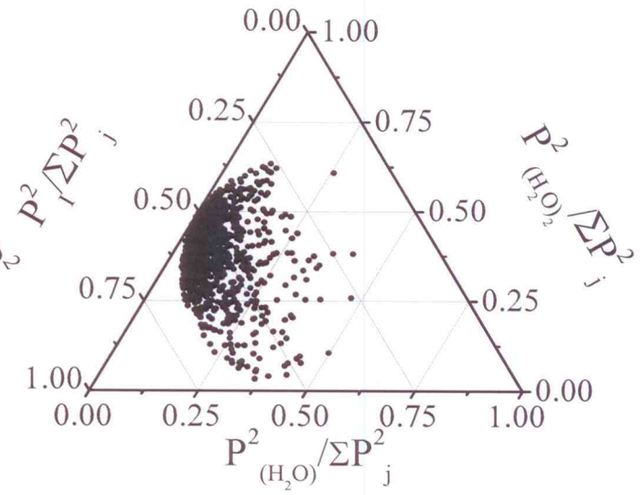

n = 3

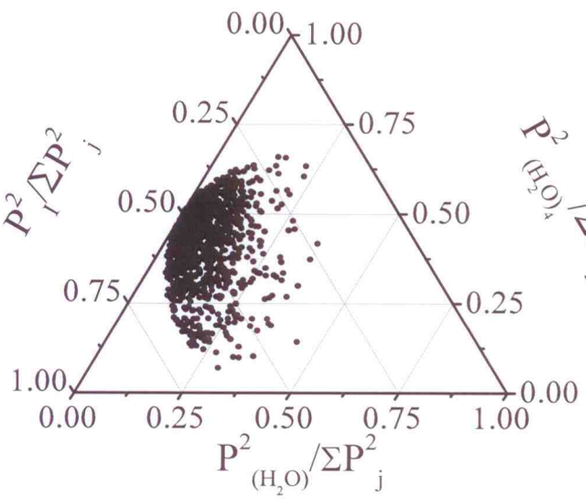

n = 4

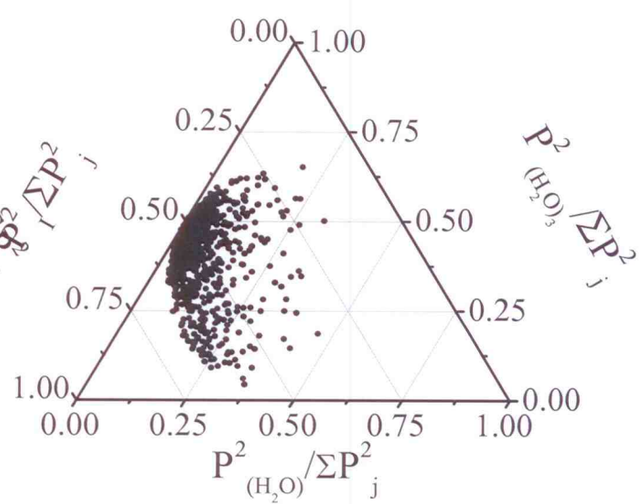

n = 5

Fig. 6